

SIMULATING SUPERNOVAE REMNANTS IN GAS CLOUDS

SIMON P. GOODWIN¹

Astronomy Centre, CPES, University of Sussex, Falmer, Brighton, BN1 9QJ

F. R. PEARCE²

Physics Department, Science Labs, University of Durham, Durham, DH1 3LE

PETER A. THOMAS³

Astronomy Centre, CPES, University of Sussex, Falmer, Brighton, BN1 9QJ

Received _____; accepted _____

¹spg@astr.cpes.susx.ac.uk

²F.R.Pearce@durham.ac.uk

³P.A.Thomas@sussex.ac.uk

ABSTRACT

The Hydra N -body hydrodynamics code has been modified to model, from the end of the Sedov phase, the effects of supernovae on the surrounding medium. The motivation is to investigate the feedback of energy into the interstellar/intergalactic medium. We compare our results for supernova remnants (SNRs) in a uniform medium to previous detailed work on the late evolution of SNRs. The code is found to reproduce the bulk characteristics of SNRs well. Results on the effects of a single central SNR on Plummer clouds are presented. The feedback of kinetic energy and the percentage mass loss can be parameterised in terms of the cloud mass and characteristic radius in a simple way.

The kinetic energy fraction returned to the ISM from a SNR is < 3 per cent. The removal of gas from the cold, dense phase and the addition of energy due to the lowering of the potential energy of a cloud is at least as significant, if not much more so, than the kinetic energy leaving a cloud.

Subject headings: supernova remnants — supernovae:general — hydrodynamics
- methods: numerical

1. INTRODUCTION

The mechanism by which energy and metals are fed back into the inter-stellar medium (ISM) by the supernovae of massive stars is an interesting and complex problem with applications to many areas of astrophysics. In this paper we present an adaptation of the Hydra N -body hydrodynamics code (Couchman, Thomas & Pearce 1995) which is capable of modelling the effects of multiple interacting supernovae over a large range of scales.

Hydrodynamical simulations of galaxy evolution and cosmological structure formation have recently been a topic of particular interest (eg. Katz 1992; Katz, Hernquist & Weinberg 1992, 1999; Navarro & White 1993; Steinmetz & Muller 1995; Frenk et al. 1996; Pearce et al. 1999). Feedback from supernovae appears to be required to reheat gas and prevent the ‘cooling catastrophe’ (White & Rees 1978; White & Frenk 1991), caused because cooling is very efficient in small halos where the cooling time is less than the dynamical time. As the particle mass in a simulation increases, more and more of these halos are resolved and a greater fraction of the available gas cools, in contradiction with the observation that only a small fraction of baryonic material is in the form of stars or cold gas. Presently the efficiency at which energy is returned to the ISM and beyond to the intergalactic medium (IGM) is a free parameter with little more than handwaving arguments to support the values adopted (eg. Katz 1992; Navarro & White 1993; Mihos & Hernquist 1994; Gerritsen & Icke 1997). It is to be expected that such efficiency parameters depend upon the density and metallicity of the surrounding gas at the very least. One of the main aims of this project is to better constrain the values of these feedback parameters (the amount of energy and material returned to the ISM as well as the spatial extent and form of the feedback) for a wide range of stellar systems.

An understanding of the early evolution of star clusters requires knowledge of how the residual gas, left within a cluster after star formation has occurred, is expelled (eg.

Tenorio-Tagle et al. 1986; Goodwin 1997a, b). Such an understanding would also help provide constraints on the initial conditions and formation models of star clusters (Goodwin 1997b). Within a larger context, information on the effects of multiple supernovae is required to construct detailed stimulated star formation models.

Much detailed work (both hydrodynamic simulations and analytic calculations) has been carried out upon the dynamics of individual supernovae expanding into a uniform ISM (see Lozinskaya 1992 and references therein), however, little of this work has concentrated upon the late phases of that expansion (exceptions including Cioffi, McKee & Bertschinger 1988; Slavin & Cox 1992; Thornton et al. 1998). Even less has been published on the effects of supernovae in gas clouds; analytic calculations were made of the effects of multiple supernovae on gas clouds by Dopita & Smith (1986) and Morgan & Lake (1989), but due to the complexity of the problem the treatment was understandably simplistic. More recently Petruk (1999a, b) has published simulations of the very early evolution of a SNR in a density gradient.

In this paper we describe the extensions we have made to the Hydra code to model this problem and present a number of convergence tests that we have performed. We also compare the results from this code to previous analytic and simulation work on individual supernovae. In section 2 we describe the testing of the code and show that it replicates the behaviour of a supernova remnant expanding into a uniform medium as studied by other authors. In section 3 we study the effects of a central supernova in Plummer clouds of various masses and characteristic radii. In section 4 conclusions are drawn and the future applications of the code detailed.

2. TESTING

In this section we present the code we have used and test both its self-consistency and its ability to reproduce known results for the evolution of SNRs in a uniform density ISM. Firstly we outline the modifications to the Hydra code. Then we show that the evolution of the energy content of an SNR and its expansion law is in good agreement with other simulations. We show that these laws hold for different ambient densities and that the properties of an SNR scale with its initial radius.

We do this to show that we are confident of the code’s ability to model the evolution of a SNR when applied to the problems of SNR evolution in a cloud in Section 3 (and in future papers).

2.1. Hydra

The public release version of Hydra, upon which the code used in this work is based, has been extensively tested in a variety of astrophysical fields (Couchman 1991, Couchman, Thomas & Pearce 1995, Thacker et al. 1999, Kay et al. 1999, Benson et al. 1999). It is an adaptive particle-particle, particle-mesh code that includes smoothed particle hydrodynamics (SPH) (Gingold & Monaghan 1977; Lucy 1977) to follow the gaseous component.

For this work we have chosen to use the latest public release version of Hydra, (Hydra3.0). This version incorporates a standard pairwise Monaghan type $\mathbf{r.v}$ viscosity rather than one based on the divergence of the local flow as used in earlier release versions of Hydra, because the $\mathbf{r.v}$ viscosity provides better shock capturing. We also employ the improved neighbour counting estimator as described by Thacker et al. (1999). To follow the radiative cooling of the gas we use the cooling rates calculated by Sutherland & Dopita

(1993) interpolated to the chosen gas metallicity.

In addition we have rewritten the SPH algorithm in order to perform complete neighbour counting even in low density regions. Previously, neighbour searching within Hydra was limited by the search length imposed by the size of the particle-particle grid, resulting in an uncomfortably high minimum resolved density. For our problem we wish to resolve the hot, low density gas within expanding supernovae shells and so have removed the maximum search-length restriction.

2.2. Individual supernovae

Here the mechanism for adding individual SNRs into a simulation is outlined.

The initial stages of a SNRs evolution are complex as an enriched, very high temperature gas ploughs into the surrounding ISM. We do not wish to simulate this phase of SNR evolution. In order to deal with multiple SNRs over a large range of length scales we ignore evolution prior to the onset of the late stages of evolution characterised by the pressure-driven snowplough (PDS) phase (cf Cioffi et al. 1988).

The choice of the beginning of the PDS phase as the starting point of the evolution within the code is due to a number of considerations. Firstly we wish to simulate the evolution of many SNRs in complex environments - the mass and time resolution (as well as the complex input physics) required to simulate the earlier stages of evolution are beyond our remit. Secondly, the evolution of a SNR to the PDS phase is reasonably well understood and provides a good basis for our simulations, allowing us reduce the mass resolution required to model its evolution. Lastly, the evolution of a SNR through the adiabatic Sedov phase even in a strong density contrast such as would be found in a molecular cloud is expected to be roughly spherical; significant non-spherical evolution would only be expected

in the late PDS phase (Dopita & Smith 1986). In dense environments, such as molecular clouds, the radius at which the PDS phase starts is much less than 1 pc, thus for significant non-spherical evolution during the Sedov phase the density change must be on a similarly small scale.

The early evolution of SNRs comprise a short-lived initial free-expansion phase followed by an adiabatic expansion (the Sedov phase) once the mass of swept-up material exceeds the initial ejecta mass (Spitzer 1978). We will concern ourselves only with the later stages of SNR evolution after the Sedov phase has finished.

A few $\times 10^4$ yrs after the initial supernova, the temperature of the adiabatically expanding remnant falls to the point at which cooling is efficient in the outer regions: $T \approx (5 - 6) \times 10^5$ K. At this point around half of the remnant mass forms a thin shell which expands into the ISM in a pressure-driven snowplough (McKee & Ostriker 1977; Lozinskaya 1992). It is at the point at which the PDS phase begins that we will start to simulate the evolution of SNRs.

At the beginning of the PDS phase the thermal energy E_T in the remnant is $E_T \approx 0.36E_{51}$. The temperature T_{PDS} of the interior gas is given by

$$T_{\text{PDS}} = 1.545 \times 10^{10} \frac{E_{51} \text{pc}^3}{n_0 r_{\text{PDS}}^3} \text{ K}, \quad (1)$$

typically a few $\times 10^6$ K. This leads to a value of the interior pressure in very good agreement with that of Chevalier (1974). The thin shell (containing half the mass) is at around 5×10^5 K.

Initially a supernova inputs energy into the ISM such that the thermal energy is $E_T \approx 0.72E_{\text{SN}}$ and the remainder is in the form of kinetic energy where E_{SN} is the total supernova energy, where the usual value is $E_{\text{SN}} = 10^{51}$ ergs (Chevalier 1974). By the time

a remnant enters the PDS phase, around 50 per cent of the thermal energy will have been lost (Lozinskaya 1992). The shell temperature is $(5 - 6) \times 10^5$ K and the interior pressure will have fallen to $P \approx E_{\text{SN}}/(4\pi R_{\text{PDS}}^3)$ where r_{PDS} is the radius at which the transfer to the PDS phase occurs (McKee & Ostriker 1977).

The radius r_{PDS} at which the PDS phase starts is given by Cioffi et al. (1988) as

$$r_{\text{PDS}} = 14 E_{\text{SN}}^{0.29} n_0^{-0.43} \zeta_m^{-0.143} \text{pc} \quad (2)$$

where n_0 is the ambient density in Hydrogen atoms cm^{-3} and ζ_m is related to the metallicity (for Solar metallicity $\zeta_m = 1$).

The initial velocity v_{PDS} of the shell is given by

$$v_{\text{PDS}} = 413 n_0^{0.143} E_{51}^{0.071} \zeta_m^{0.214} \text{ km s}^{-1} \quad (3)$$

These parameters (radius and velocity) are similar to those given by other authors (eg. Chevalier 1974; Falle 1981; Blondin et al. 1998). Differences are mainly due to the use of different cooling functions although the shell velocity predicted at the same radius is very similar for all calculations.

The main reasons for preferring the calculations of Cioffi et al. (1988) over other calculations are that they include a correction factor for non-Solar metallicities and their good agreement with the simulations of Thornton et al. (1998).

2.3. SNRs in the code

In the remainder of this section we compare our results for a SNR in a uniform medium with those of other authors as well as testing the convergence and self-consistency of our

results.

SNRs are set-up by taking all of the particles in a sphere of radius r_{PDS} centred on the position of the supernova. Half of the particles are unmoved but are heated up to T_{PDS} to represent the hot interior (uniform density and pressure, no bulk motions). The other half of the particles are distributed on the surface of a sphere of radius r_{PDS} and given a velocity outwards from the centre of the sphere of v_{PDS} at a temperature of 5×10^5 K.

Low particle numbers within r_{PDS} have an effect on the evolution of the SNR due to shot noise causing significant non-sphericity. Generally more than ≈ 60 particles are required within r_{PDS} to model the SNR well although as few as 20 do a reasonable job (we would not wish however to trust simulations where the included particle number is this low).

2.3.1. SNR energy

Table 1 gives the parameters used in 10 example runs covering a factor of 8 in N , 2.5 in box size and over 30 in mass resolution for the same physical initial conditions. These runs are used in the next 2 subsections to illustrate the stability of the code at reproducing results over this range of parameters and to compare with other authors to show the ability of the code to well represent the post-Sedov phase evolution of a SNR.

Figure 1 shows the change in the total energy within the simulation volume, normalised to the value at 1 Myr to take into account the different amounts of total thermal energy present in simulation volumes of varying size (in large boxes the thermal energy of the undisturbed gas is by far the largest contributor to the total energy). The ‘lost’ energy has been radiated away by the hot gas, the energy conservation being good, a maximum of 0.1 – 0.2 per cent. Good agreement is seen over a wide variety of particle mass and box size.

The small differences are mainly due to the requirement that there be an integer number of particles in the interior and shell of the SNR. This leads to small differences between the initial thermal and kinetic energies of each model which amount to a few per cent, a difference which is amplified as time progresses. For instance, the initial kinetic energy of runs 1019 and 1020 differ by 4 per cent, by 6 Myr the difference in fig. 1 of $0.02E_{51}$ represents approximately 4 per cent of the total energy change.

A more detailed examination of the energy balance for three of the SNRs is shown in fig. 2, approximately 0.6 Myr after the supernova explosion. The solid lines show the sum of the thermal and kinetic energy within each radius with the dashed and dot-dashed lines showing the total thermal and kinetic energy respectively within each radius. The outwardly moving shell is clearly visible. The differences in interior thermal energy are due to shot noise and very low particle numbers in these regions - the high thermal energies of runs 1002 and 1017 within the inner 10 pc are due to 1 hot particle. The agreement of the energies over a factor of more than 30 in mass resolution is good and is representative of all runs. The shell has a peak density at approximately 60 pc at 0.6 Myr and is wider where the mass resolution is poor.

2.3.2. SNR expansion law

The expansion of a SNR can be roughly characterised as a power law of the form $r \propto t^\nu$ (with t being measured from the time of the supernova). McKee & Ostriker (1977) find for negligible external pressure that $\nu = 2/7$ (≈ 0.286). Chevalier (1974) finds $\nu = 0.305$ for early times and for late evolution ($t > 0.75$ Myr) $\nu = 0.32$. This is close to the Cioffi et al. (1988) offset solution where $r \propto (t - t_{\text{offset}})^{0.3}$. From inspection of fig. 3 in Thornton et al. (1998), they appear to obtain a value around $\nu = 0.3$. All these values are below the power law for a purely momentum conserving snowplough where $\nu = 0.4$ (Spitzer 1978).

Figure 3 shows the evolution of the shell radius with time for the ten convergence test runs (which model the same physical conditions at different mass resolutions and box sizes) detailed in table 1. In fig. 3 the shell radius is determined by the mean radial distance from the centre of the SNR of the densest particles. At low shell radii r this is less reliable due to the smaller number of particles in the shock (especially when the mass resolution is poor).

The best fit to the first 1.5 Myr of evolution is shown by the dashed curve fitted with;

$$r(t) = r_{\text{PDS}} \left(\frac{t}{t_{\text{PDS}}} + 1 \right)^\nu \quad (4)$$

with r in pc and t in Myr (t is the simulation time, ie. the time since the onset of the PDS phase), t_{PDS} is of order the duration of the PDS phase. Leaving r_{PDS} , t_{PDS} and ν as free parameters the best fit is given by $r_{\text{PDS}} = 18.34$ pc, $t_{\text{PDS}} = 0.012$ Myr and $\nu = 0.317$. For an $n_0 = 0.5 \text{ cm}^{-3}$ ISM, r_{PDS} is actually 18.85 pc (from eqn. 2) and $t_{\text{PDS}} = r_{\text{PDS}}/v_{\text{PDS}}$ is around 0.02 Myr (Cioffi et al. 1988).

The late stages (> 1.5 Myr) are well fitted by the solid line, $r = 55.8 + 16.8t$, a reasonably good fit to free expansion of a sound wave, the sound speed in this case of 15.6 pc Myr^{-1} .

2.3.3. *Different ambient densities*

We have investigated the differences in SNR evolution within ISMs of different ambient densities. Table 2 shows the range of ambient densities tested, covering 4 orders of magnitude. Previous studies (with the exception of Thornton et al. 1998) have concentrated on investigating low ambient densities representative of the ISM in the Solar neighbourhood.

Figure 4 shows the shell evolution for the range of densities presented in table 2. Also

shown is the radius and time at which the shell velocity falls to the sound speed for each density.

From the data presented in table 2 the radius at which the sound speed is reached is fitted by a power-law in density of $r_{\text{sound}} = 65n_0^{-0.37}$ pc and the time by a power-law of the form $t_{\text{sound}} = 1.2n_0^{-0.38}$ Myr.

These power-law fits to r_{sound} and t_{sound} are almost exactly what are expected. Using eqn. 4 and the known dependencies on n_0 of $r_{\text{PDS}}(\propto n_0^{-0.43}$ - eqn. 2) and $t_{\text{PDS}}(\propto r_{\text{PDS}}/v_{\text{PDS}} \propto n_0^{-0.57}$ - eqns. 2 & 3) gives for $t/t_{\text{PDS}} \gg 1$

$$r \propto n_0^{-0.25} t^{0.32} \tag{5}$$

as $v_{\text{sound}} = r_{\text{sound}}/t_{\text{sound}} = \text{constant}$ leads to the predictions that $t_{\text{sound}} \propto n_0^{-0.36}$ and $r_{\text{sound}} \propto n_0^{-0.37}$, very close to the fitted relations from the simulations.

The initial energy (thermal and kinetic) of the SNR and the evolution of the total energy is approximately the same for each density if the evolution of a SNR through the PDS phase is scaled so that the radial properties are in units of r_{PDS} as illustrated in fig. 5. The radial total, thermal and kinetic energies are plotted against r/r_{PDS} for 3 models spanning a range of 4 orders of magnitude in density for the time when $r_{\text{shell}} \approx 2 \times r_{\text{PDS}}$. For $n_0 = 0.01 \text{ cm}^{-3}$, $2r_{\text{PDS}} \approx 200 \text{ pc}$, for $n_0 = 0.5 \text{ cm}^{-3}$, $2r_{\text{PDS}} \approx 38 \text{ pc}$ while for $n_0 = 100 \text{ cm}^{-3}$, $2r_{\text{PDS}} \approx 3.9 \text{ pc}$.

As is clear in fig. 5 the energy profiles of the SNRs in terms of r/r_{PDS} are very similar, indeed the main differences are due to the fact that the output radii shown are not exactly $r_{\text{shell}} = 2 \times r_{\text{PDS}}$ but differ by a few per cent (due to the finite number of outputs).

When $r = 2 \times r_{\text{PDS}}$ the mass of the hot interior is around twice the interior mass at the onset of the PDS phase as most of the swept-up material remains in the dense shell.

The interior temperature falls by a factor of around 2.7 while the shell temperature has fallen to $\approx 10^4$ K. The shell velocity has fallen by a factor of 5 (as expected if v scales as $v_{\text{PDS}}(t/t_{\text{PDS}} + 1)^{-0.68}$, cf. eqn. 4). The scaling of the SNR properties with r_{PDS} across all densities is because the energy content of SNRs is density independent - a doubling of the volume of the SNR will result in the same energy changes throughout the SNR independent of the ambient density (as swept-up mass dominates).

2.3.4. Late-starting SNRs

Figure 6 shows the late evolution of three SNRs, two started at the onset of the PDS phase and the other started at $r = 2 \times r_{\text{PDS}}$ with $T_{\text{shell}} = 10^4$ K and the interior temperature given by $T_{\text{SNR}} = 0.37 \times T_{\text{PDS}}$ (where T_{PDS} is given by eqn. 1) and $v_{\text{shell}} = 0.2v_{\text{PDS}}$. The total energy within the late-starting SNR is very similar to that in those that started at r_{PDS} but the relative contributions of the kinetic and thermal energies within the bubble are slightly different. This is due to the shorter amount of time which the $2r_{\text{PDS}}$ simulation has had to convert bulk motions into thermal energy within the bubble. Again the main differences between the simulations are due to outputs not being at exactly the right times. The ability to start modelling each SNR at $2 \times r_{\text{PDS}}$ will become very useful when we wish to add SNRs to massive gas clouds reducing the required mass resolutions in simulations by a factor of 8 (see section 3).

2.3.5. Metallicity effects

The effect of different metallicity environments can be significant during the early evolution of SNRs, during the PDS phase however the differences due to metallicity are found to be negligible (see also Thornton et al. 1998). Initially a metallicity of $\zeta_m = 0.01$

will make a factor of 1.93 difference in r_{PDS} and 0.37 in v_{PDS} as compared to a $\zeta_m = 1$ SNR (from eqns. 2 & 5 respectively). However, the effect of these different initial SNR conditions is not as significant as it might first appear, because the velocity of a $\zeta_m = 1$ SNR at $r = 1.93 \times r_{\text{PDS}}(\zeta_m = 1)$ is $\approx 0.22v_{\text{PDS}}(\zeta_m = 1)$ (see above) resulting in only slightly different expansions.

The subsequent evolution of SNRs with different metallicities through the PDS phase are virtually indistinguishable (as also found by Thornton et al. 1998). The evolution of the shell radii is slightly different at early times due to different values of r_{PDS} but as mentioned above this difference is soon nearly cancelled out and at late times the shell radii differ by only a few pc. When SNRs are started with the same r_{PDS} but different metallicities the difference is negligible. The evolution of the total energies within each SNR are also remarkably similar. Differences in metallicity affect the cooling of the hot interior and hence the pressure and the extra driving force on the shell. However, during expansion into a uniform ambient medium the shock acceleration is dominated by the deceleration due to the sweeping-up of material, making metallicity (which effects the pressure-driven acceleration) a minor factor in the late-time evolution of the SNR.

The differences in energy between different metallicities are accounted for by the different initial conditions at the onset of the PDS phase however it is not clear that even the early stages of SNR evolution would be affected by low-metallicity effects. A type II supernova with a progenitor mass of $25M_{\odot}$ will produce around $2.4M_{\odot}$ of heavy metals (Tsujiimoto et al. 1995), the majority ($1.8M_{\odot}$) being O^{16} . In the case of a SNR expanding into an ISM of density $n_0 = 100 \text{ cm}^{-3}$ (where the mass within r_{PDS} is $\approx 75.5M_{\odot}$) this will enrich the swept-up material from $\zeta_m = 1$ (Solar) to $\zeta_m = 2.6$ and from $\zeta_m = 0.01$ to $\zeta_m = 1.6$. Such enrichment is very significant and will alter the evolution of the pre-PDS phases. However, by $5r_{\text{PDS}}$ the amount of swept-up material is $9440M_{\odot}$ and has been

enriched from $\zeta_m = 0.01$ to $\zeta_m = 0.023$, a fairly insignificant (from the point of view of cooling) amount. Thornton et al. (1998) did not find a significant effect when including the metals ejected from the supernova (Thornton 1999). Obviously this enrichment and its history is of vital importance for understanding chemical evolution, and the enrichment history can be followed by this code (once a number of assumptions about mixing have been included), but it has little bearing on the late-time evolution of an individual SNR in a uniform medium.

2.3.6. Computational aspects

The softening included in the simulations does not greatly affect the results of the shell expansion and energy transfer. Similar runs differing in softening are virtually indistinguishable in their results (two such runs, differing by a factor of over 4 in softening - 1002 & 1005 - are included in fig. 1). The softening selected for simulations should be as small as is reasonably practicable given that the smallest region in which results can be believed in detail is no less than the softening length, which also determines the width of any shock fronts that are present. Unfortunately the number of timesteps required rises as the softening length is decreased.

The width of the shell that forms the snowplough is difficult to determine accurately as it becomes slightly aspherical as it evolves due to initial Poisson fluctuations in the particle positions. This effect is worse for the models which began with only a few particles in the SNR. When spherically averaged profiles are produced this leads to an artificial broadening of the snowplough and general smoothing of the steep shock fronts. The snowplough width is expected to be a few pc (Thornton et al. 1998), in these simulations the shock width is approximately the softening.

2.4. Summary

In this section we have shown that the code is stable and converges for reasonable selections of box size and particle mass. The code is able to reproduce the results of other authors for the situation of a SNR expanding into a uniform ambient medium during the PDS phase of evolution. In the next section we will place SNRs in the centres of Plummer model gas clouds.

3. CENTRAL SUPERNOVAE IN A GAS CLOUD

While the evolution of a SNR in a uniform density ISM provides a good test of the ability of the code to reproduce the characteristics of a SNR as found in more detailed hydrodynamic calculations, it is not physically realistic. The effects of a supernovae in a stratified medium (eg. a gas cloud) is a more practical problem. Massive stars are found in young clusters, their lifetimes being so short that they are expected to still be embedded in gas remaining from star formation. The significant evolution of a young SNR is therefore expected to occur in the confines of its parent GMC. Massive stars are also found to be centrally-concentrated in clusters (Hillenbrand 1997; Carpenter et al. 1997) so that an investigation of a central SNR is a good approximation to the evolution of the first SNR in a cluster.

Some analytic calculations of the effects of supernovae in a gas cloud have been made by Dopita & Smith (1986) and Morgan & Lake (1989) to estimate the number of supernovae required to totally disrupt a gas cloud of a given mass. Morgan & Lake (1989) using more detailed cooling functions than Dopita & Smith (1986) found that the minimum mass of a $(1/r^2)$ cloud for it to confine a single central supernova was $4 \times 10^4 M_{\odot}$.

As noted in section 2.3, Dopita & Smith (1986) find that a SNR within the high-density

environment of a gas cloud will remain roughly spherical during the adiabatic phase of its evolution. Using this result we may place SNRs in the cloud at the start of the PDS phase in the same way as they are placed in the uniform medium simulations. The high densities in gas clouds ($n_0 > 10^4 \text{ cm}^{-3}$) means that the adiabatic phase will end whilst the shell radius is very small ($\ll \text{pc}$).

Cloud initial conditions are based on a Plummer model ($n = 5$ polytrope) with mass distribution;

$$M(r) = \frac{Mr^3}{R^3} \frac{1}{[1 + r^2/R^2]^{3/2}} \quad (6)$$

where M is the total mass and R is the scale length. The half-mass radius of a cloud is then $\approx 1.3R$. Clouds are constructed out to a maximum radius r_{max} of a few R (normally $r_{\text{max}} = 20 \text{ pc}$), resulting in the actual mass being slightly less than M .

In this paper we will only deal with Plummer model clouds. Obviously the effects of a SNR will depend, at least to some extent and possibly very significantly, upon the density distribution of the parent cloud. These will be dealt with in detail in a paper to follow.

Observationally, Giant Molecular Clouds (GMCs) can be approximated very roughly by clouds with $M = \text{a few } \times 10^4 \text{ to a few } \times 10^5 M_\odot$ and $R = \text{a few pc}$ (eg. Harris & Pudritz 1994) which we used as initial conditions for our simulations (full details in table 3). Before inserting any supernovae, our clouds are allowed to relax to a stable state in which they are virialised. Support is provided by the thermal energy of the gas and the bulk kinetic energy is negligible (although the temperature of the gas represents the turbulent velocity which supports the cloud rather than the molecular temperature). The clouds are self-gravitating as are real giant molecular clouds (Rivolo & Solomon 1988) and so require no pressure confinement from an external hot diffuse gas.

The insertion of a supernova has the effect of adding considerable amounts of kinetic and thermal energy to the cloud. By the end of the Sedov phase, the extra energy amounts to around 6.4×10^{50} ergs, comparable to or greater than the potential energy of the system (roughly $8.6 \times 10^{40} (M/M_\odot)^2 / (R/\text{pc})$ ergs). The shock from the supernova then passes through the the cloud.

3.1. Some numerical considerations

The number of particles within r_{PDS} required for the SNR evolution to be a good approximation to more complex simulations is > 40 with > 60 giving the best results (see section 2). For a Plummer model cloud the central density is

$$\rho_0 = \frac{3M}{4\pi R^3} \quad (7)$$

where M is the mass of the cloud and R is the Plummer scale length. Using equation 2 the mass interior to r_{PDS} at the cloud core will be

$$M_{\text{PDS}} \approx 5.48 \frac{R_{\text{pc}}^{6/7}}{M_5^{2/7}} M_\odot \quad (8)$$

where $R_{\text{pc}} = R/\text{pc}$ and $M_5 = M/10^5 M_\odot$ (we shall be using R_{pc} and M_5 throughout the rest of this section). We require a mass resolution at least 60 times smaller than this giving, for $R_{\text{pc}} = 3.5$ and $M_5 = 1$ a minimum particle number of $N > 3.74 \times 10^5$.

Such resolutions, while attainable, require significant computing time to run. Our aim here is to introduce SNRs in such a way as to allow many simulations covering a variety of initial conditions to be completed, so as to explore the parameter space. Starting SNR evolution at $r = 2 \times r_{\text{PDS}}$ (see Section 2.3.4) allows a factor of 8 reduction in the mass

resolution and therefore the number of particles required to model the cloud. In the case of a $10^5 M_\odot$ cloud 2×32^3 particles are required, on a workstation each timestep takes around 3 minutes resulting in a 20 Myr simulation in around 30 hours.

3.2. Feedback as a function of cloud structure

Here we present the analysis of the energy and mass feedback as a function of M_5 and R_{pc} , the cloud models are presented in table 3. Initially all clouds are virialised and particles are said to be lost once they cross the box edges which are a distance $2r_{\text{max}}$ from the centre of the cloud (at a distance roughly equal to the tidal radius of a GMC). It is these lost particles that comprise the feedback from the cloud into the larger ISM. In most cases the SNRs are started at $2r_{\text{PDS}}$.

As a 'standard' model we use the run with parameters $M_5 = 1$, $R_{\text{pc}} = 3.5$ to illustrate the general features of SNR evolution in a Plummer cloud. Initially the cloud has 0.0356×10^{51} ergs of thermal energy and a potential energy of -0.0711×10^{51} ergs. The SNR starting at $2r_{\text{PDS}}$ adds a total of 0.123×10^{51} ergs of kinetic energy and 0.289×10^{51} ergs of thermal energy (calculated from section 2) creating a net positive energy for the system of 0.38×10^{51} ergs.

3.2.1. The evolution of the SNR

The evolution of the shell velocity with radius for the standard model is shown in fig. 7. It is typical of all runs that the velocity drops from its initial value (v_{PDS} or $0.2v_{\text{PDS}}$ of started at $2r_{\text{PDS}}$) reaching a minimum value v_{min} at around 2 to 3 R_{pc} before accelerating to around $1.5 \times v_{\text{min}}$ on leaving the box.

It is found later that v_{\min} and associated quantities may be used to parameterise all of the effects of a SNR on a gas cloud. In this subsection we sketch a model of the SNR evolution that predicts v_{\min} in terms of the two cloud parameters M_5 and R_{pc} .

The velocity reaches v_{\min} when the acceleration due to the interior pressure matches the deceleration due to the sweeping-up of material. The force on the shell due to pressure $F_{\text{press}}(r)$ goes as

$$F_{\text{press}} = (4\pi r^2)P \quad (9)$$

where P is the pressure when the shell radius is $r(t)$.

The initial radius of the shell (r_{PDS}) is very small compared to R and as adiabatic cooling goes as $(r_{\text{PDS}}/r)^5$ the majority of the cooling will be adiabatic, especially at late times so

$$P \approx P_{\text{PDS}} \frac{r_{\text{PDS}}^5}{r^5} \quad (10)$$

with P_0 given by $\rho_0 k T_{\text{PDS}}$ (where ρ_0 is the central density $\propto M_5/R_{\text{pc}}^3$). The initial temperature T_{PDS} is given by eqn. 1 as

$$T_{\text{PDS}} \propto \frac{M_5^{0.29}}{R_{\text{pc}}^{0.87}} \quad (11)$$

The force due to the sweeping-up of material (momentum conservation) $F_{\text{mom}}(r)$ is

$$F_{\text{mom}}(r) = (4\pi r^2)\rho(r)v(r)^2 \quad (12)$$

equating eqns. 9 and 12 using eqn. 10 gives

$$\rho(r_{\min})v_{\min}^2 = P_0 \frac{r_{\text{PDS}}^5}{r_{\min}^5} \quad (13)$$

using eqn. 11 and assuming that $r_{\min} \gg R$ gives

$$v_{\min} \propto \frac{R_{\text{pc}}^{0.29}}{M_5^{0.93}} \quad (14)$$

Fitting the powers of M_5 and R_{pc} simultaneously gives a best linear fit to v_{\min} of

$$v_{\min} = 6.58 \frac{R_{\text{pc}}^{0.32}}{M_5^{0.77}} \text{ km s}^{-1} \quad (15)$$

which is compared to the simulations in fig. 9. The similarities between eqns. 14 and 15 are remarkable considering the very simple assumptions that went into the formulation of eqn. 14.

The accelerating force due to the pressure goes as r^{-5} and so rapidly becomes negligible at high r . It is still able, however, to increase the velocity of the shell by the time it leaves the cloud to $\approx 1.5v_{\min}$.

The above rather simplistic treatment avoids (as is necessary) many details of the actual SNR evolution in a cloud. In the simulations the main shell of the SNR is followed by a weaker shock which is created by the shocking of infalling material filling the interior when it reaches the centre (and meets other infalling material). This creates a very complex density/pressure structure in the cloud as the SNR evolves.

We now go on to show how the effects of a SNR on a cloud can be parameterised very simply in terms of v_{\min} and closely related quantities.

3.2.2. Metallicity effects

As the temperature factor T_0 is so important in setting the value of v_{\min} , then metallicity, Z , is an important factor in that in clouds of lower Z than the fiducial Solar $Z = 1$, cooling will be less efficient and T_0 and v_{\min} higher. In the case of a $Z = 0.01$ metallicity cloud the kinetic energy lost increases to 2.5×10^{49} ergs and the mass lost to $5.4 \times 10^4 M_{\odot}$, a 67 per cent increase on the $Z = 1$ cloud in both cases. For a $Z = 0.1$ cloud the increase in both values is 46 per cent. This would indicate that the effects of the first generation of supernovae would have been much more dramatic than those which occurred later once metal enrichment had taken place.

3.2.3. Mass loss and disruption

The mass loss from the cloud would be expected to be related the escape velocity from the cloud at the point where the minimum velocity is reached. The escape velocity at $2R_{\text{pc}}$ is given by $18.6\sqrt{M_5/R_{\text{pc}}}$ km s⁻¹ and it is found that if $v_{\min} > v_{\text{esc}}(r_{\min})$ then the cloud completely disrupts, ie. all of the mass is lost. At the other extreme if $v_{\min} < 0.2v_{\text{esc}}(r_{\min})$ then no mass loss (and hence no feedback) occurs. In the intermediate regime the mass loss is related to $v_{\text{esc}}(r_{\min})$ by

$$\frac{M_{\text{lost}}}{M_5} = 0.25 \times \left(\frac{v_{\min}}{v_{\text{esc}}}\right)^{2.5} \quad (16)$$

as illustrated in fig. 10.

3.2.4. Energy feedback

The amount of energy returned to the ISM from a cloud would be expected to be related to the kinetic energy of the cloud at v_{\min} given by $T_{\min} = 1/2 M_{\text{shell}} v_{\min}^2$ where M_{shell} is the mass of the shell at r_{\min} , most simply we might expect $M_{\text{shell}} \propto M_5$.

Illustrated in fig. 11 is the feedback energy from table 3 against $T_{\min}/10^{51}$ ergs $= 0.001 M_5 (v_{\min}/\text{km s}^{-1})^2$. Two linear regimes are obvious in the behaviour of the feedback energy. In the upper limit where the cloud has totally disrupted the feedback energy is fitted by

$$E_{\text{lost}} = -0.0012 + 0.25 M_5 v_{\min}^2 \times 10^{51} \text{ ergs} \quad (17)$$

in the lower limit where the mass loss is negligible the feedback energy is

$$E_{\text{elost}} = -0.012 + 0.25 M_5 v_{\min}^2 \times 10^{51} \text{ ergs} \quad (18)$$

as can be easily seen the slope of these two relationships is the same and the constant factor, different by exactly one order of magnitude, is the only difference. The intermediate stage marks the change from the total cloud destruction and high feedback to the low mass loss and low feedback regime. This region is only a very small region of the total $M_5 - R_{\text{pc}}$ parameter space.

3.2.5. The final state of clouds

As stated above when $v_{\min} > v_{\text{esc}}$ a single SNR is enough to disrupt a cloud completely and when $v_{\min} < 0.2 v_{\text{esc}}$ no mass loss occurs at all. In the intermediate regime some gas is retained in a bound object - a new cloud with lower mass than the original.

The ratio of the final to initial potential energy, Ω_f/Ω_i is related again to the ratio of the minimum velocity of the shell and the escape velocity v_{\min}/v_{esc}

$$\frac{\Omega_f}{\Omega_i} = 1.26 - 1.05 \frac{v_{\min}}{v_{\text{esc}}} \quad (19)$$

as illustrated in fig. 12. This relationship is only valid for $0.3 < v_{\min}/v_{\text{esc}} < 1$, beyond 1 the cloud is totally destroyed and $\Omega_f/\Omega_i = 0$ and less than 0.3 Ω_f/Ω_i asymptotes to 0.

The change in potential energy of a gas cloud due to a central supernova can sometimes be significantly more important than the feedback of kinetic energy as illustrated in table 3. Clouds lose all of their initial potential energy if they are completely disrupted. If the cloud loses only part of its mass then the significant energy change occurs as a loss of potential energy from the cloud (a net gain of energy). Even when no mass loss or feedback occurs a small change (of the order of a few percent) in the potential energy is observed as the cloud expands slightly.

As fig. 13 shows, the remaining material settles back into a new configuration that can also be described as a Plummer model with a lower central density and larger scale length. Thus knowing the initial mass M and characteristic radius R gives the final characteristic radius R_f via;

$$R_f = \left(1 - \frac{M_{\text{lost}}}{M}\right)^2 R \left(\frac{\Omega_f}{\Omega_i}\right)^{-1} \quad (20)$$

Knowing the final mass and characteristic radius of the cloud allows the effects of further central supernovae on that cloud to be calculated - as long as the interval between supernovae is greater than the time required for the cloud to relax to a new equilibrium.

The time taken for a $5 \times 10^5 M_{\odot}$ cloud to recover from a central supernova is very short, the majority of the SNR's kinetic and thermal energy is radiated away in $< 1\text{Myr}$. Assuming

a Salpeter IMF, the number of massive stars within a cloud that will go supernovae is $N_{\text{SNe}} \approx 0.006M\epsilon$ where M is the mass of the cloud and ϵ is the star formation efficiency. Taking $\epsilon = 0.01$ and $M = 5 \times 10^5 M_{\odot}$ gives $N_{\text{SNe}} = 30$. If these supernovae occur centrally and evenly spaced over a 30 Myr period then no ejecta will escape the cloud and the cloud will not be disrupted by the SNRs.

These results hold for Plummer model clouds that can be characterised solely by M and R . This study will be extended to other density distributions in a future paper which we are preparing.

4. CONCLUSIONS

The Hydra N -body SPH code has been extended to allow the simulation of the evolution of supernova remnants (SNRs) from the onset of the pressure-driven snowplough (PDS) phase. In section 2 this code was seen to be able to produce convergent results over a wide range of parameter space and reproduce the results on the evolution of SNRs from a variety of previous authors. The power of this code is the ability to simulate the evolution of SNRs in a variety of environments using a workstation in a reasonable time (of the order of days).

This code represents the first time that we are able to model multiple, interacting SNRs in gas clouds and complexes. This paper is the first detailed analysis of SNR evolution in a gas cloud to examine the feedback parameters so important in galaxy formation and evolution calculations.

In section 3 we presented new results on the effect of a single, central supernova on Plummer model gas clouds of various masses and characteristic radii. The results of Dopita & Smith (1986) and Morgan & Lake (1989) were found to be too simplistic. The

evolution of a central SNR is very complex, the late stages of evolution are governed by pressure-driving from a hot interior accelerating the SNR shell down the density gradient.

Feedback from a cloud is defined to be the mass and energy which pass out of our simulation box (whose size is approximately the tidal radius of the cloud). The results may be summarised as:

- The efficiency of energy feedback, mass loss and cloud destruction for a central supernova in a Plummer cloud of mass M and characteristic radius R is related to the minimum velocity v_{\min} that the shock reaches during it's evolution. This minimum velocity is given by $v_{\min} = R_{\text{pc}}^{0.32}/M_5^{0.77}$.
- For $v_{\min} > v_{\text{esc}}$ the cloud is totally destroyed, while for $v_{\min} < 0.2v_{\text{esc}}$ the SNR is completely contained and no feedback occurs.
- The mass lost from a cloud is related to the ratio of the minimum velocity to the escape velocity v_{\min}/v_{esc} as $M_{\text{lost}}/M = 0.25(v_{\min}/v_{\text{esc}})^{2.5}$.
- The energy feedback E_{lost} has two main regimes with equal slopes where $E_{\text{lost}} = -C_E + 0.25M_5V_{\min}^2 \times 10^{51}$ ergs where $C_E = 0.0012$ when $v_{\min}/v_{\text{esc}} > 1.1$ and $C_E = 0.012$ when $v_{\min}/v_{\text{esc}} < 0.9$.
- The loss of (negative) potential energy is often the largest (positive) increase of energy in the system and at least of order the feedback of kinetic energy, the feedback of thermal energy being negligible in comparison to both.
- The final state of a cloud that is not destroyed is close to a Plummer model with final characteristic radius R_f related to the initial parameters by $R_f = (1 - M_{\text{lost}}/M)^2 R(\Omega_f/\Omega_i)^{-1}$.

- The efficiency of feedback increases rapidly with decreasing metallicity suggesting that feedback at early epochs was far more efficient.

Our simulations are obviously not perfect. The code takes no account of magnetic fields (following standard astrophysical practice) which may well be important, especially at late times. In addition the feedback from massive stars into the cloud before they become supernovae is neglected, although in the dense environments of cloud cores we may be justified in ignoring this effect (Franco, García-Segura & Plewa 1996). A simple method of including such effects in the code is being developed. Despite this we believe that this code represents a significant step in modelling the effects of multiple SNRs on clouds and the larger ISM.

4.1. Future directions

As noted in the introduction, a code such as this has many interesting applications. It can be used to investigate how gas clouds of different sizes and shapes are affected by internal supernovae, calculating the feedback of energy and mass into the ICM. We are in the process of preparing papers that will expand the current work into an investigation of off-centre SNRs in gas clouds and of the effect of different density distributions on feedback parameters.

In addition we will be able to investigate how the cloud is disrupted and in what way gas is expelled on a small scale. This has important consequences for investigating the early evolution of star clusters. A paper is in preparation on the effects of gas expulsion on the dynamics of the stellar content of a cluster and what star formation efficiency is required for a bound object to remain.

Using supercomputers $N = 10^7$ or more is possible, giving the resolution to model fully

the dynamical and chemical evolution of a dwarf galaxy. In addition feedback can be placed into simulations of the formation of the first cosmological objects.

ACKNOWLEDGMENTS

PAT is a PPARC Lecturer Fellow. We would like to thank Hugh Couchman for useful discussions about this paper and acknowledge NATO CRG 970081 which facilitated this interaction. We would also like to thank Anne Green and Roger Hutchings for their help. This project was completed using the computer facilities of the University of Sussex Astronomy Centre and University of Sussex BFG computer using the Hydra code (public release version available from the Hydra Consortium at http://phobos.astro.uwo.ca/hydra_consort/).

In memory of Jenny.

REFERENCES

- Benson, A. J., Pearce, F. R., Jenkins, A., Cole, S., Baugh, C., Frenk, C. S. & Lacey, C., in preparation
- Blondin, J. M., Wright, E. B., Borkowski, K. J. & Reynolds, S. P. 1998, *ApJ*, 500, 342
- Carpenter J. M., Meyer, M. R., Dougados, C., Strom, S. E., & Hillenbrand, L. A. 1997, *AJ*, 114, 198
- Chevalier, R. A. 1974, *ApJ*, 188, 501
- Cioffi, D. F., McKee, C. F. & Bertschinger, E. 1988, *ApJ*, 334, 252
- Couchman, H. M. P. 1991, *ApJ*, 368, L23
- Couchman, H. M. P., Thomas, P. A. & Pearce, F. R. 1995, *ApJ*, 452, 797
- Dopita, M. A. & Smith, G. H. 1986, *ApJ*, 304, 283
- Evrard, A. E., Metzler, C. A. & Navarro, J. F. 1996, *ApJ*, 469, 494
- Falle S. A. G. E. 1981, *MNRAS*, 195, 1011
- Franco J., García-Segura G. & Plewa T. 1996, astro-ph/9609140
- Frenk, C. S., Evrard, A. E., White, S. D. M. & Summers, F. 1996, *ApJ*, 472, 460
- Gerritsen, J. P. E. & Icke, V. 1997, *A&A*, 325, 972
- Gingold, R. A. & Monaghan, J. J. 1977, *MNRAS*, 181, 375
- Goodwin, S. P. 1997a, *MNRAS*, 284, 785
- Goodwin, S. P. 1997b, *MNRAS*, 286, 669

- Harris, W. E. & Pudritz, R. E. 1994, *ApJ*, 429, 177
- Hillenbrand, L. A. 1997, *AJ*, 1997, 113, 1733
- Katz, N. 1992, *ApJ*, 391, 502
- Katz, N., Hernquist, L. & Weinberg, D. H. 1992, *ApJ*, 399, L109
- Katz, N., Hernquist, L. & Weinberg, D. H. 1999, *ApJ*, in press
- Kay, S. T., Pearce, F. R., Jenkins, A., Frenk, C. S., White, S. D. M., Thomas, P. A. & Couchman, H. M. P. 1999, submitted *MNRAS*
- Lozinskaya, T. A. 1992, 'Supernovae and Stellar Wind in the Interstellar Medium', (AIP: New York)
- Lucy, L. B. 1977, *AJ*, 82, 1013
- McKee, C. F. & Ostriker, J. P. 1977, *ApJ*, 218, 148
- Mihos, J. C. & Hernquist, L. 1994, *ApJ*, 437, 611
- Morgan, S. & Lake, G. 1989, *ApJ*, 339, 171
- Navarro, J. F. & White, S. D. M. 1993, *MNRAS*, 265, 271
- Pearce, F. R., Jenkins, A., Frenk, C. S., Colberg, J. M., White, S. D. M., Thomas, P. A., Couchman, H. M. P., Peacock, J. A. & Efstathiou, G., 1999, in press *ApJL*
- Petruk O. 1999a, *A&A*, 344, 295
- Petruk O. 1999b, *A&A*, 346, 961
- Rivolo, A. R. & Solomon, P. M. 1988, in 'Molecular Clouds in the Milky Way and External Galaxies', ed. Dickman, Snell & Young, *Lecture Notes in Physics* Vol. 315, p42

Slavin, J. D., & Cox, D. P. 1992, ApJ, 392, 131

Spitzer, L. 1978, Physical Processes in the Interstellar Medium (PUP: Princeton)

Steinmetz, M., & Müller, E., 1995, MNRAS, 276, 549

Sutherland, R. S. & Dopita, M. A. 1993, ApJS, 88, 253

Thacker, R. J., Tittley, E. R., Pearce, F. R., Couchman, H. M. P. & Thomas, P. A., 1999,
submitted MNRAS

Thornton, K., Gaudlitz, M., Janka, H.-Th. & Steinmetz, M. 1998, ApJ, 500, 95

Thornton, K. 1999, private communication

Tenorio-Tagle, G., Bodenheimer, P., Lin, D. N. C. & Noriega-Crespo, A. 1986, ApJ, 221, 635

Tsujimoto, T., Nomoto, K., Yoshii, Y., Hashimoto, M., Yanagida, S. & Thielemann, F.-K.
1995, MNRAS, 277, 945

White, S.D.M. & Frenk, C.S., 1991, ApJ, 379, 52

White, S.D.M. & Rees, M.J., 1978, MNRAS, 183, 341

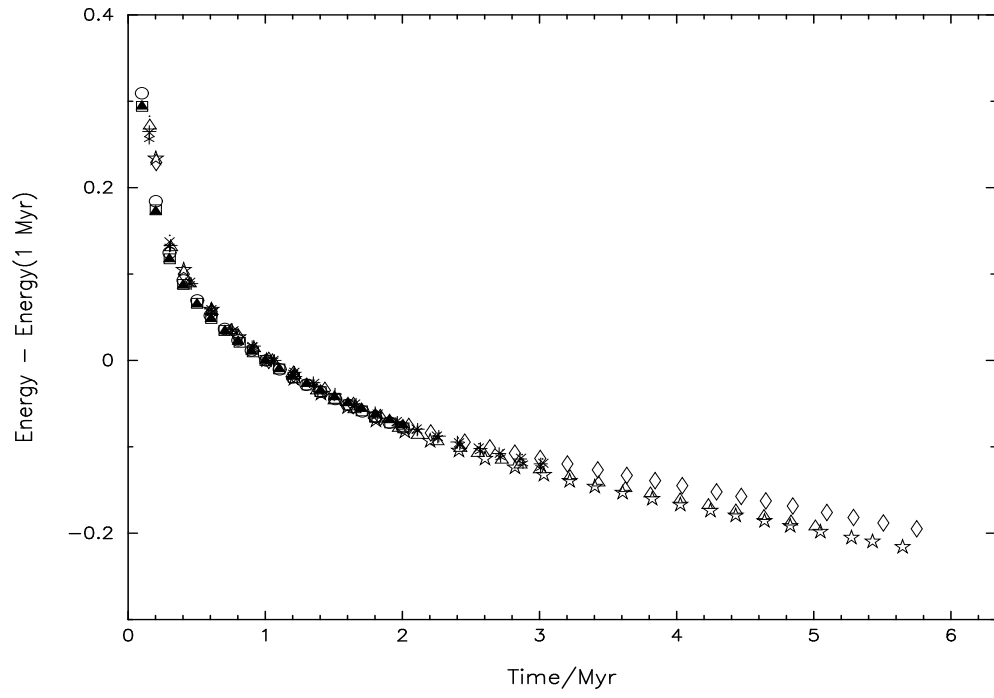


Fig. 1.— The change in the total energy with time for the ten SNRs detailed in table 1 normalised to the total energy within the simulation volume at 1 Myr in units of 10^{51} ergs. The ‘lost’ energy has been radiated away.

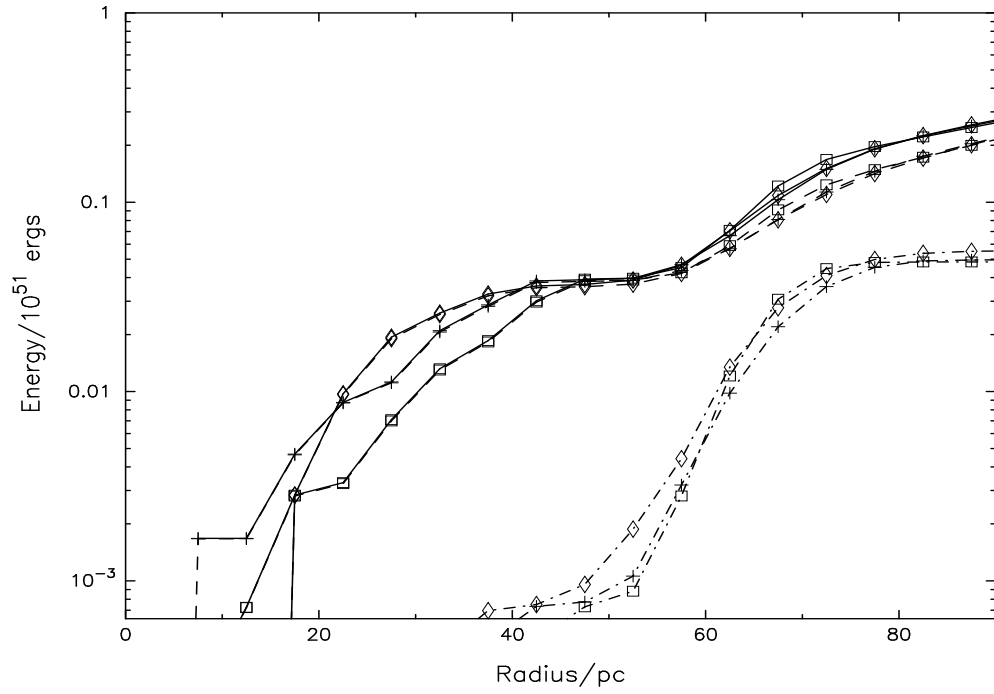


Fig. 2.— The energy balance for the SNRs in runs 1002 (cross), 1017 (square) and 1019 (diamond) at 1 Myr. The solid lines show the sum of the thermal and kinetic energy, the dashed lines show the thermal and the dash-dot line the kinetic energy within each radius.

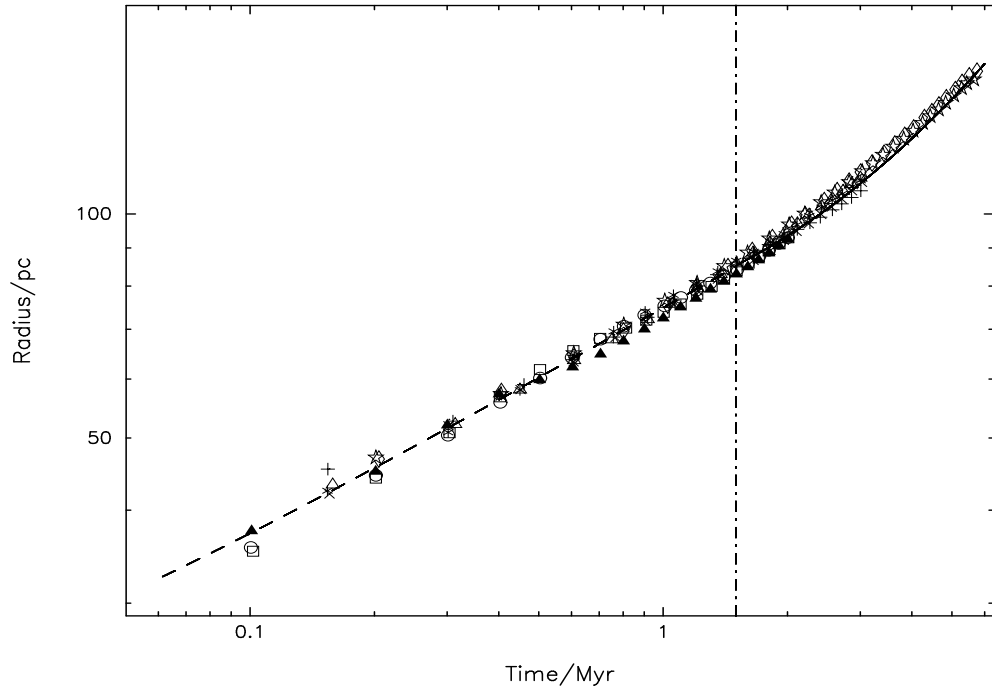


Fig. 3.— The evolution of the shell radius with time for the ten convergence runs detailed in table 1. The fits to different evolutionary stages are explained in the text. The rough region of transition from the radiative pressure driven snowplough phase to the constant expansion phase is indicated by the dashed line at 1.5 Myr.

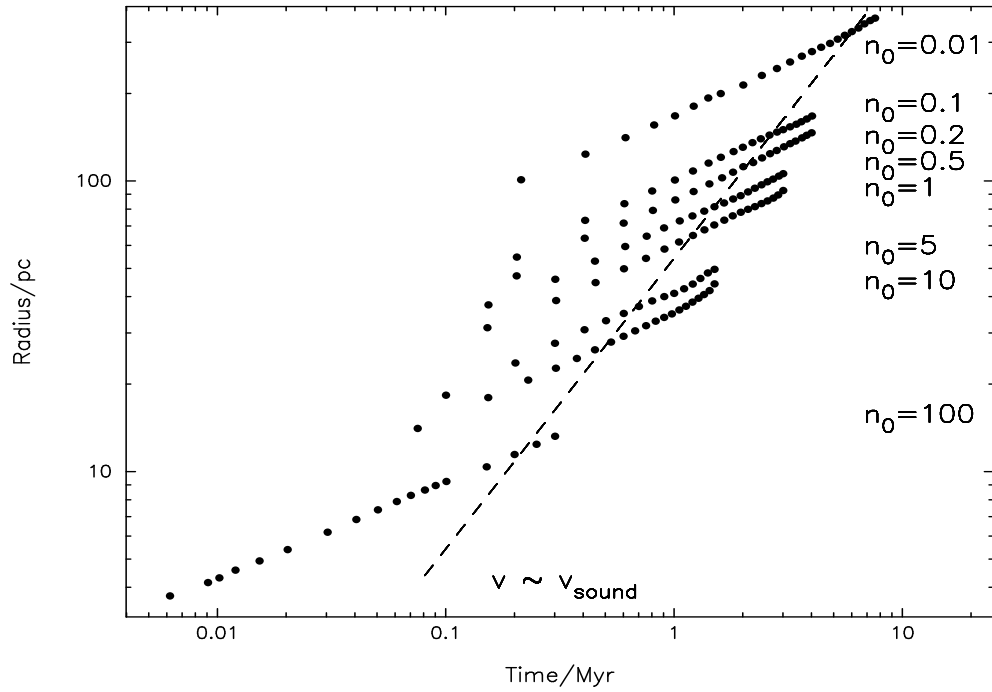


Fig. 4.— The evolution of the shell radius for 8 different ambient density ISMs all at 10^4 K detailed in table 2. The hydrogen atom density per cm^3 is marked by each track. The approximate time and radius at which the shell velocity falls to the ISM sound speed (and the tracks become curved) is marked by the dashed line.

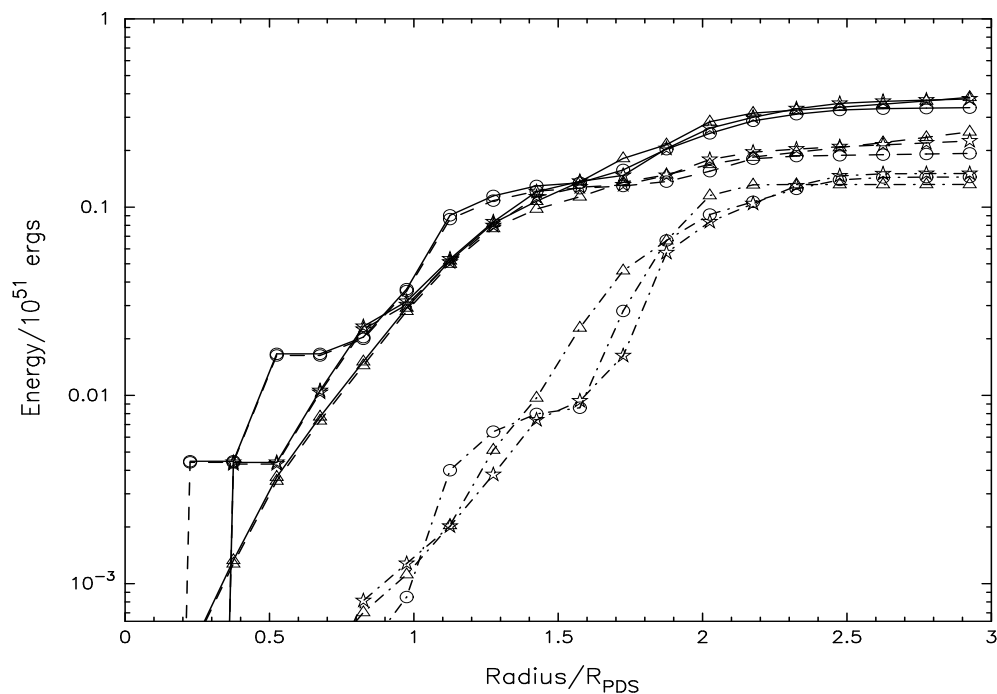


Fig. 5.— The total (solid line), thermal (dashed line) and kinetic (dot-dash line) energies within each radius at a shell radius of $\approx 2 \times r_{\text{PDS}}$ the radial distribution being given in terms of r/r_{PDS} for three different densities of $n_0 = 0.01 \text{ cm}^{-3}$ (triangles), $n_0 = 0.5 \text{ cm}^{-3}$ (stars) and $n_0 = 100 \text{ cm}^{-3}$ (circles).

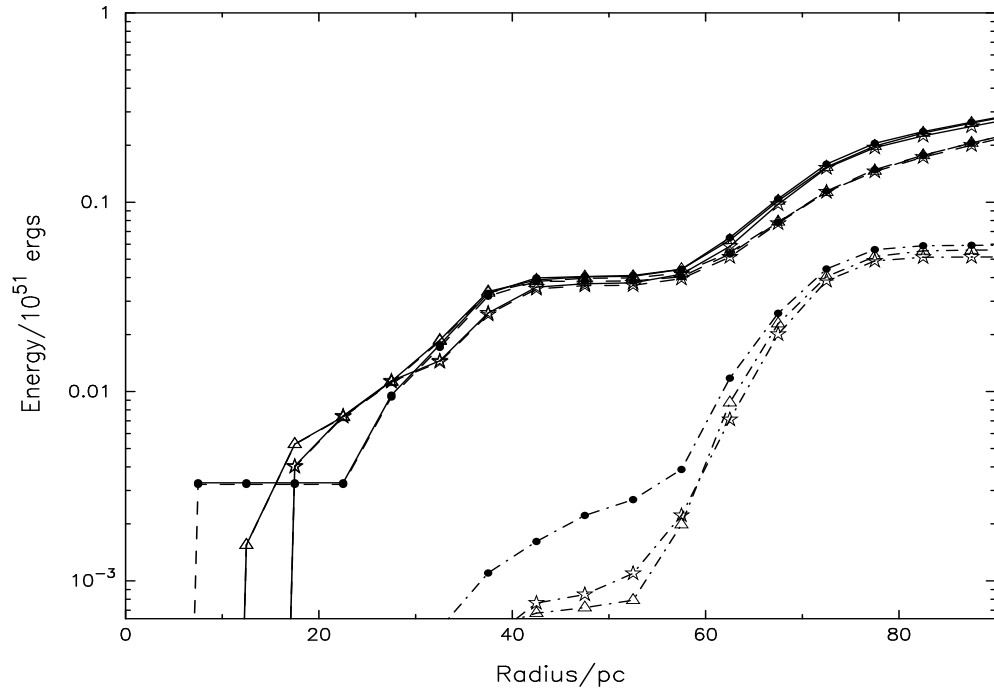


Fig. 6.— The radial energy profiles of runs 1003 (stars) and 1018 (triangles) at 1 Myr compared to that of a run started at $r = 2 \times r_{\text{PDS}}$ (circles). The shell radius at this time is ≈ 55 pc. The energies shown are the total (full line), thermal (dashed line) and kinetic (dot-dash line) within each radius.

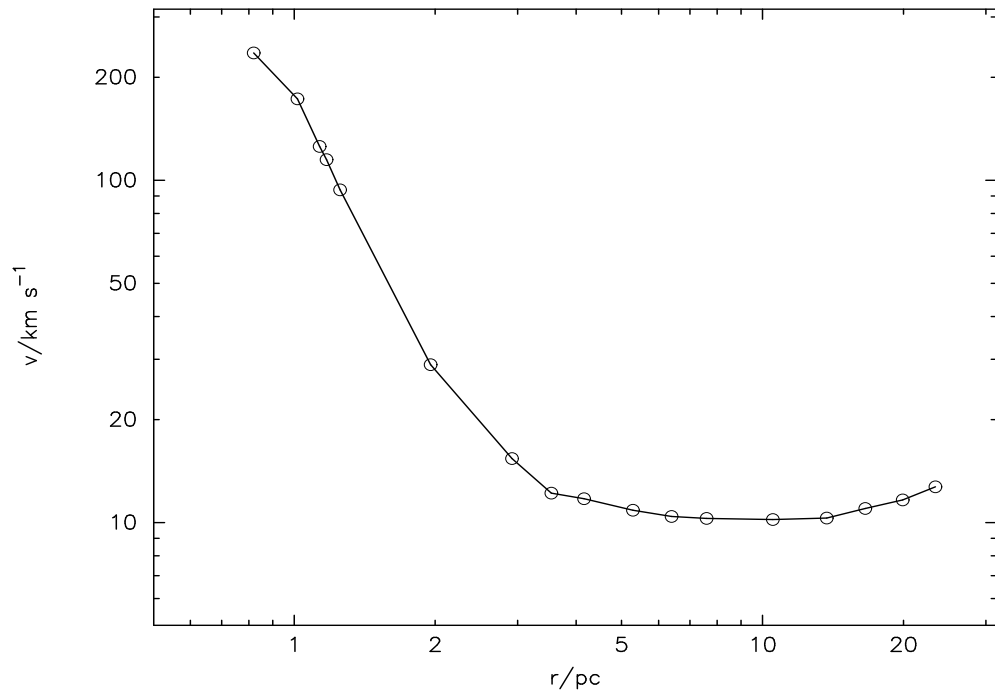


Fig. 7.— The evolution of the shock velocity with radius for the standard $M_5 = 1$, $R = 3.5$ cloud.

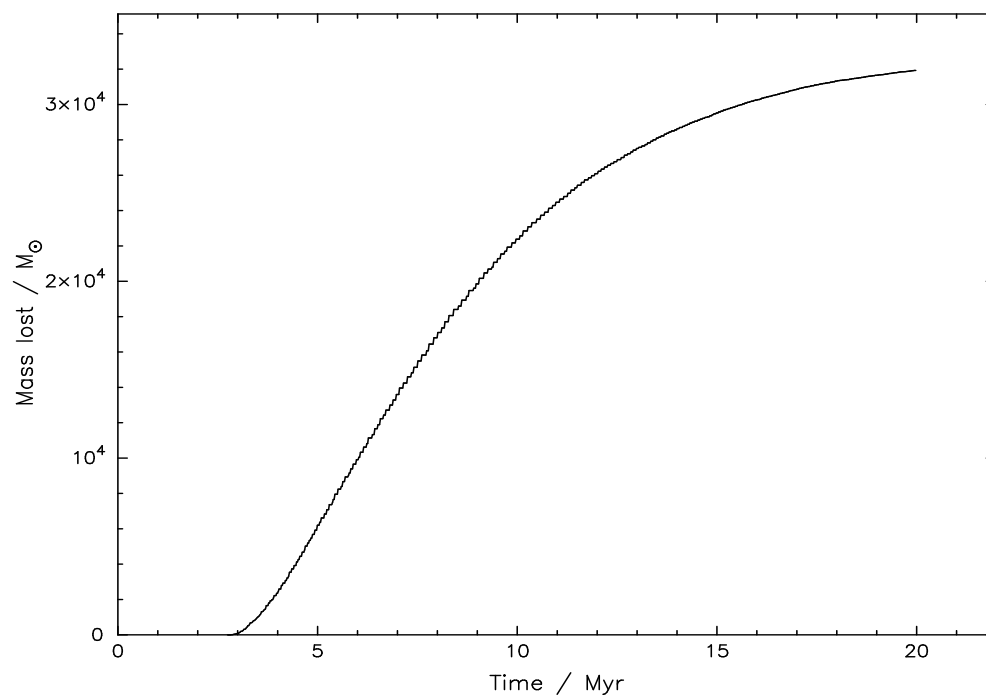


Fig. 8.— The mass loss rate across the sides of the simulation cube with time for a $M = 10^5 M_{\odot}$, $R = 3.5$ pc, $r_{\max} = 20$ pc Plummer cloud with a central supernovae.

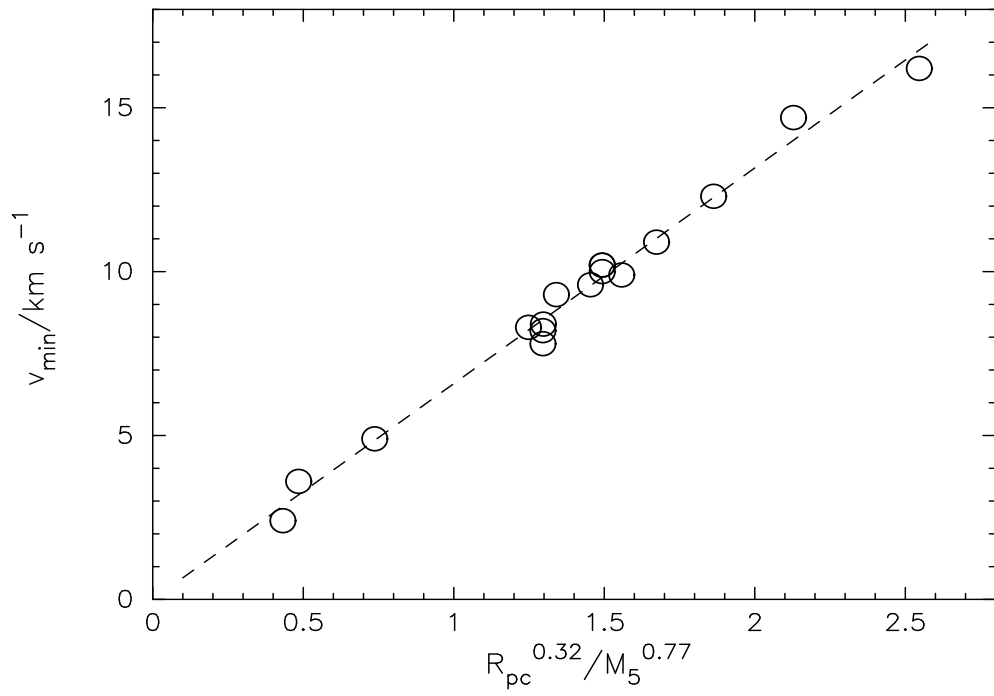


Fig. 9.— The minimum shock velocity v_{\min} in km s^{-1} against the Plummer cloud characteristics $R_{\text{pc}}^{0.32}/M_5^{0.77}$ from eqn. 15.

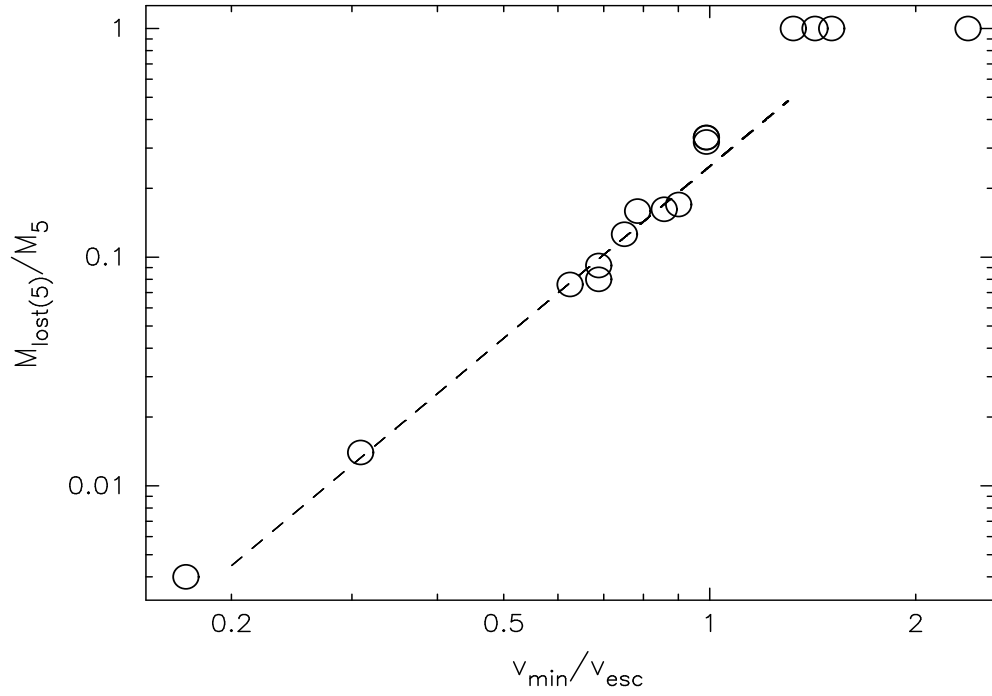


Fig. 10.— The fractional mass lost against the ratio of the minimum velocity to escape velocity for the Plummer clouds listed in table 3. A fit from eqn. 16 is added for clouds with $0.2v_{\text{esc}} < v_{\min} < v_{\text{esc}}$ (clusters with partial mass loss - see text).

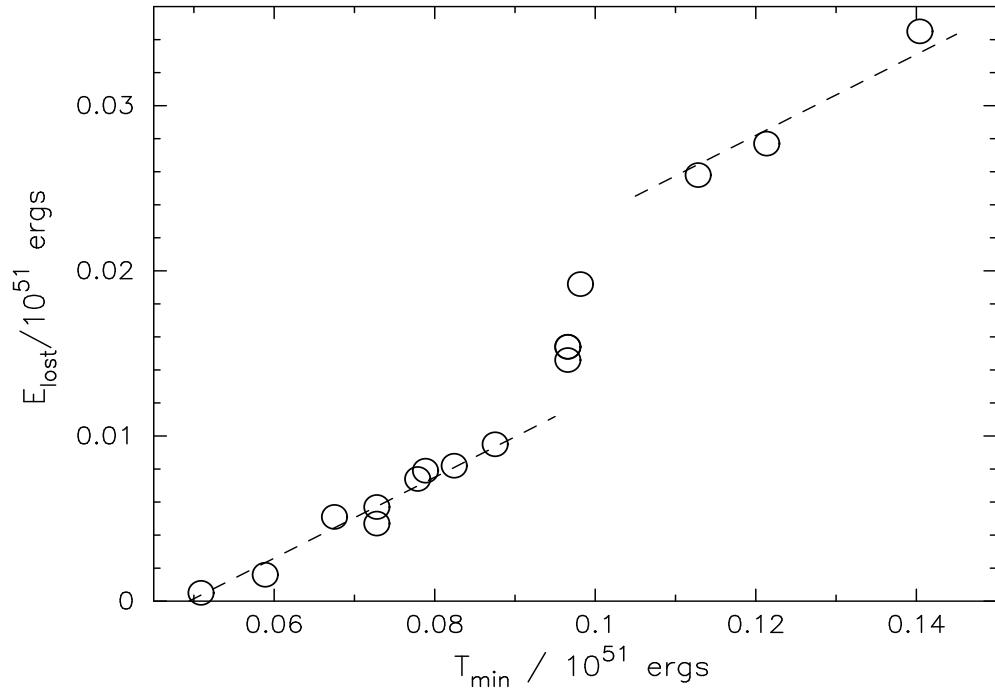


Fig. 11.— The feedback energy E_{lost} against the minimum kinetic energy parameter $T_{\min} = 0.001M_5(v_{\min}/\text{km s}^{-1})$. Linear fits of the same slope are fitted from eqns. 17 & 18 are marked by dashed lines.

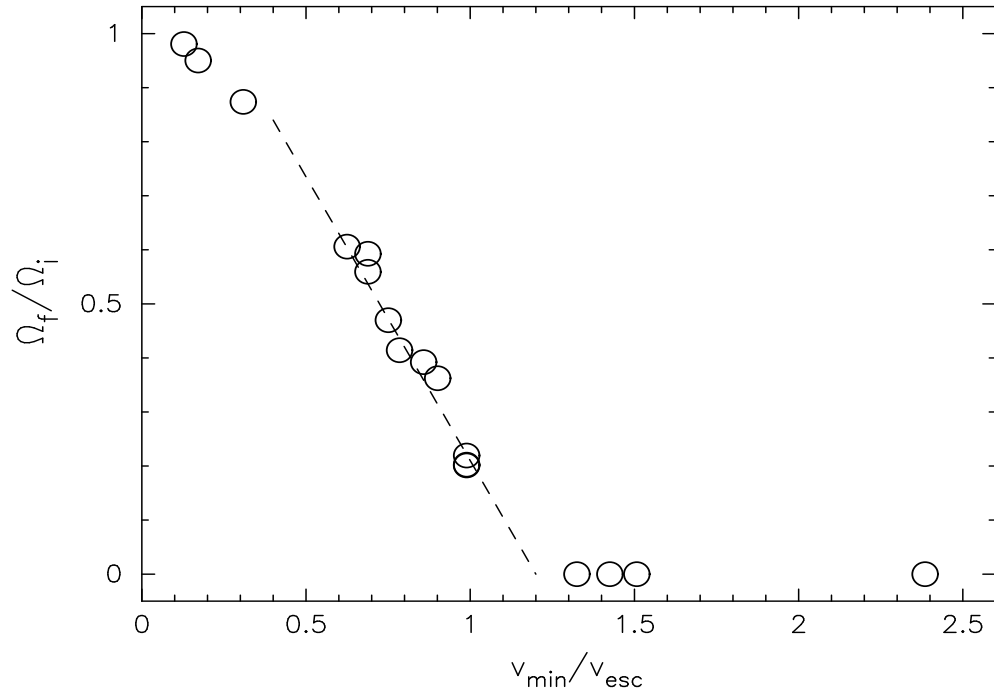


Fig. 12.— The final-to-initial potential energy ratio against the ratio of the minimum velocity to escape velocity for the Plummer clouds listed in table 3. The linear relationship marked by the dashed line is from eqn. 19.

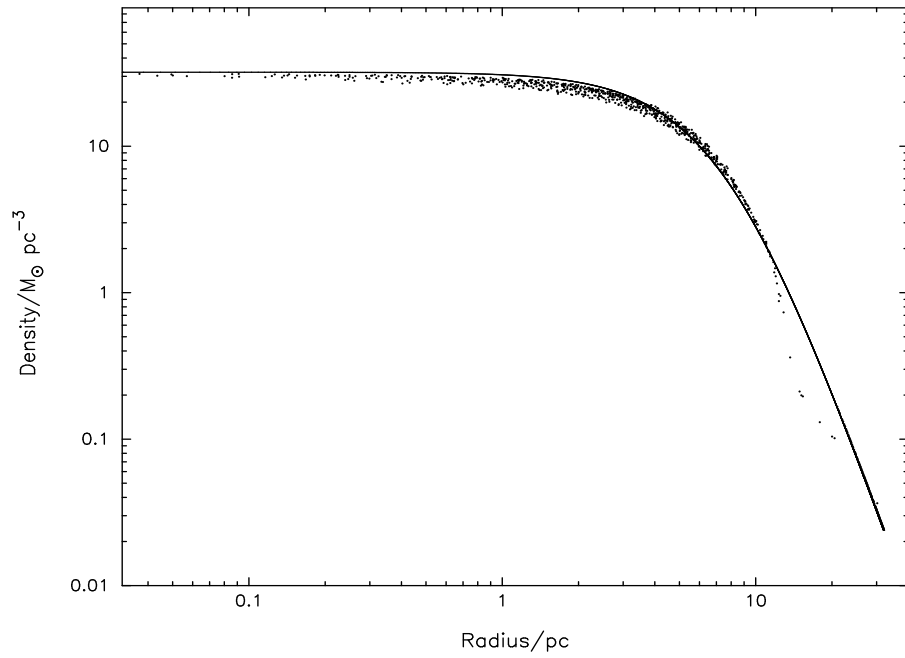


Fig. 13.— The density distribution after 20 Myr for the $10^5 M_{\odot}$ Plummer cloud from fig. 8. The solid line is a Plummer model with $M = 6.36 \times 10^4 M_{\odot}$ and $R = 7.8 \text{ pc}$

Table 1. Parameters of the ten $n_0 = 0.5 \text{ cm}^{-3}$, $\zeta_m = 1$ convergence test runs. The table gives the run identification number, box size (in pc), softening (in pc), number of particles N , the end time of the simulation (in Myr), the mass of an individual particle (in M_\odot) and the symbol used to represent each run in figs. 1,2,3 and 6.

RUN	box pc	softening pc	N	End time Myr	Particle mass M_\odot	Symbol
1001	300	27	32^3	3	11.1	dot
1002	300	23	2×32^3	3	5.53	cross
1003	300	18	4×32^3	3	2.77	star
1004	300	5	64^3	2	1.38	circle
1005	300	5	2×32^3	3	5.53	'x'
1017	200	11	4×32^3	2	0.82	square
1018	400	20	4×32^3	5	6.56	triangle
1019	500	28	4×32^3	6	12.8	diamond
1020	500	22	64^3	6	6.40	open star
1021	200	9	64^3	2	0.41	open cross

Table 2. The density of the surrounding ISM, the initial radius of the PDS and the approximate time and radius at which the shell velocity falls below the ambient medium’s sound speed. The evolution of the shell radius with time for the different ambient densities used here is plotted in fig. 4.

RUN	n_0 cm^{-3}	r_{PDS} pc	t_{sound} Myr	r_{sound} pc
1006	0.01	101	7.2	360
1007	0.1	38	3.0	150
1008	0.2	28	2.2	120
1003	0.5	18	1.6	84
1009	1	14	1.3	66
1010	5	7.0	0.70	37
1011	10	5.2	0.45	26
1012	100	1.9	0.21	11

Table 3. The cloud models and feedback parameters of the runs in Section 3. The Plummer parameters mass M_5 and radius R_{pc} for each cloud are followed by the minimum velocity v_{min} of the shell in that cloud, the fractional mass loss M_{lost}/M , the energy feedback E_{lost} and the loss of potential energy Ω_{lost} from that cloud.

M $10^5 M_{\odot}$	R pc	v_{min} km s $^{-1}$	M_{lost}/M	E_{lost} 10^{48} ergs	Ω_{lost} 10^{48} ergs
0.5	2	14.7	1.00	19	32
0.5	3.5	16.2	1.00	35	18
0.75	2	9.9	0.17	7.9	45
0.75	3.5	12.3	1.00	26	40
0.9	2.5	9.6	0.16	8.2	50
1	2	8.3	0.076	5.1	50
1	2.25	7.8	0.080	4.7	45
1	2.25	8.2	0.092	5.7	49
1	2.5	9.3	0.13	7.4	53
1	3.5	10.2	0.33	15	57
1	3.5	10.0	0.32	15	56
1	3.5	10.2	0.33	15	57
1	5	10.9	1.00	28	49
1.2	3.5	8.4	0.16	9.5	60
2.5	3.5	4.9	0.014	1.6	56
5	3.5	2.4	0	0	34
5	5	3.6	0.004	0.5	62